Orientation and Alignment Echoes

G. Karras,[1] E. Hertz,[1] F. Billard,[1] B. Lavorel,[1] J.-M. Hartmann,[2] and O. Faucher[1,*]
[1]*Laboratoire Interdisciplinaire CARNOT de Bourgogne, UMR 6303 CNRS-Université de Bourgogne, BP 47870, 21078 Dijon, France*

[2]*Laboratoire Interuniversitaire des Systèmes Atmosphériques (LISA) CNRS (UMR 7583), Université Paris Est Créteil, Université Paris Diderot, Institut Pierre-Simon Laplace, Université Paris Est Créteil, 94010 Créteil Cedex, France*

Erez Gershnabel, Yehiam Prior, and Ilya Sh. Averbukh[†]
Department of Chemical Physics, The Weizmann Institute of Science, Rehovot 76100, Israel
(Received 27 January 2015; published 15 April 2015)

We present one of the simplest classical systems featuring the echo phenomenon—a collection of randomly oriented free rotors with dispersed rotational velocities. Following excitation by a pair of time-delayed impulsive kicks, the mean orientation or alignment of the ensemble exhibits multiple echoes and fractional echoes. We elucidate the mechanism of the echo formation by the kick-induced filamentation of phase space, and provide the first experimental demonstration of classical alignment echoes in a thermal gas of CO_2 molecules excited by a pair of femtosecond laser pulses.

DOI: 10.1103/PhysRevLett.114.153601 PACS numbers: 42.50.Md, 37.10.Vz, 45.50.-j

Echoes are common in many areas of physics. When an inhomogeneous ensemble of many nonlinear systems is impulsively kicked by an external force, the transient response to the kick vanishes fast due to dispersion in the properties of individual systems. The same happens when the ensemble is kicked again; however, a new impulsive response shows up at twice the delay between the two pulses—a celebrated echo phenomenon first observed by Hahn in precessing nuclear spins [1]. Echoes have been observed in a wide class of classical systems, including cyclotron echo [2,3], plasma wave echo [4], photon echo [5] and its mechanical analogs [6]. Echoes were predicted to occur in proton storage rings [7,8], and were observed in high energy hadron beam experiments [9,10]. Echo-enabled generation of short-wavelength radiation in free-electron lasers [11–13] was demonstrated (for a recent review, see Ref. [14]). Echoes are being also discussed in the context of cavity quantum electrodynamics [15,16] and cold atom systems [17–20].

In this Letter, we identify one of the simplest classical systems featuring the echo phenomenon—a collection of free classical rotors stimulated by an external impulsive force. Using geometric arguments on the kick-induced transformations of the rotors' phase space, we predict multiple echoes in the mean orientation or alignment of the ensemble. Our qualitative analysis reveals the echo mechanism and predicts its dependence on parameters of the stimulating kicks. A full analytical theory of these echoes in 2D and 3D thermal ensembles of classical rotors, and its generalization to the quantum case will be published elsewhere [21]. Here, we discuss the physics behind the predicted echo effect and demonstrate it experimentally in a collection of CO_2 molecules stimulated by a pair of femtosecond laser pulses.

For a linear molecule having a permanent dipole moment μ, and driven by a linearly polarized field, the interaction potential leading to orientation is $V(\theta,t) = -\mu E(t)\cos(\theta)$, where $E(t)$ is the field amplitude and θ is the polar angle between the molecular axis and the field direction. In the absence of a permanent dipole moment, the external field couples to the induced molecular polarization. For non-resonant laser fields, the angular-dependent interaction potential is $V(\theta,t) = -(\Delta\alpha/4)E^2(t)\cos^2(\theta)$ [22,23], which leads to alignment along the field polarization (for reviews on molecular alignment see Refs. [24–28]). Here $\Delta\alpha$ is the polarizability anisotropy, and $E(t)$ is the envelope of the laser pulse. The effects we present here are rather similar for the above two interaction types. Thus, in what follows, we use the dipole interaction form ($V \sim -\cos(\theta)$) for discussion, and point out differences appearing in the case of alignment [$V \sim -\cos^2(\theta)$].

Consider an ensemble of 2D rotors kicked by a short orienting pulse at $t = 0$. The angular velocity ω and angle θ of a rotor at time t are given by

$$\omega = \omega_0 - \Omega\sin(\theta_0), \qquad \theta = \theta_0 + \omega t. \tag{1}$$

Here ω_0, θ_0 are the initial conditions, and Ω is proportional to the intensity of the kick. The orientation of the ensemble of rotors is quantified by the mean value $\langle\cos(\theta)\rangle$, referred to as the orientation factor. Let us first assume that all the rotors are initially at rest and uniformly distributed in the angular interval $[-\pi,\pi]$, as represented by the horizontal blue line in Fig. 1. A short kick in the $\theta = 0$ direction does

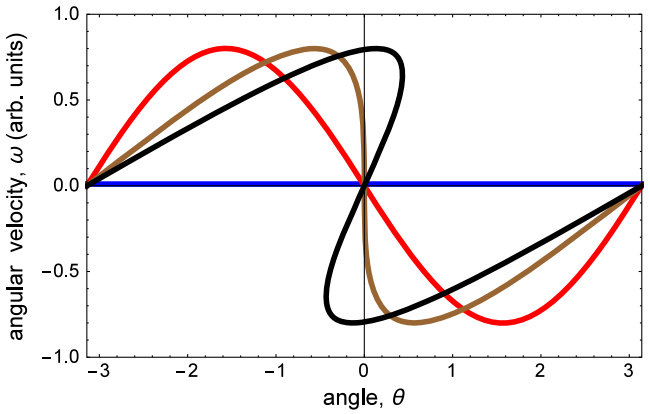

FIG. 1 (color online). Kick-induced orientation of an ensemble of rotors (see text for details).

not move the rotors during its action, but induces rotation with angular speed $-\Omega\sin(\theta)$ [see Eq. (1)]. Immediately after the kick, the phase space distribution of the rotors takes a shape shown by the red curve in Fig. 1. In the course of the following free evolution, each point on the red curve moves horizontally towards $\theta = 0$ with a velocity defined by its initial vertical position, as shown by the next two curves. After a certain delay, the curve experiences steepening at $\theta = 0$ (brown curve), not unlike the accumulation of cars in congested traffic, which leads to a singularity in the angular distribution of the rotors [29]. Note, however, that the maximal value of the orientation factor $\langle\cos(\theta)\rangle$ is achieved not at this moment, but some time later, when the curve takes a typical folded shape (black curve in Fig. 1) leading to an increased density of rotors in the region near $\theta = 0$ [29]. This is a transient orientation, and the stronger the kick the shorter is the time needed to reach the maximally oriented state.

Next, we consider an ensemble that is initially uniformly dispersed in angle, and has a spread in angular velocity ω. For certainty, we assume a Gaussian distribution of angular velocities $f(\theta_0,\omega_0)\sim\exp[-\omega_0^2/(2\sigma^2)]$. The time-dependent orientation factor after the kick is found to be $\langle\cos(\theta)(t)\rangle = \exp[-\sigma^2t^2/2]J_1(\Omega t)$, where $J_1(z)$ is the Bessel function of the first order. This pulsed response disappears fast as $\sigma t\to\infty$. By inverting the map (1) and using its area preserving property, one arrives at the following expression for the probability distribution function at time t:

$$f(\omega,\theta,t)=\frac{1}{2\pi}\frac{1}{\sqrt{2\pi}\sigma}\exp\left[-\frac{[\omega-\Omega\sin(\omega t-\theta)]^2}{2\sigma^2}\right]. \quad (2)$$

Figure 2 shows the transformation of the initial distribution with time. Shortly after the kick [Fig. 2(a)] the density distribution takes a folded shape similar to the one shown in Fig. 1, resulting in the transient orientation. On the longer time scales, when the orientation signal $\langle\cos(\theta)\rangle(t)$ vanishes,

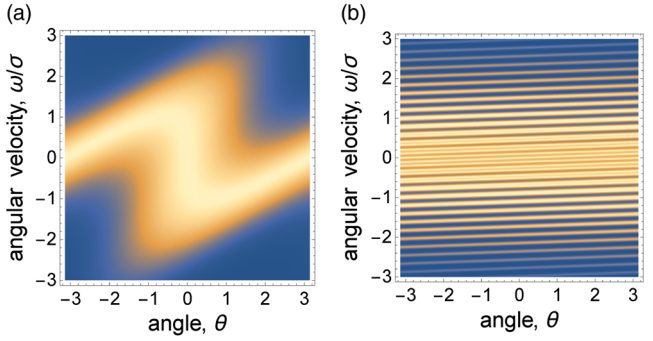

FIG. 2 (color online). Filamentation of the phase space density distribution. $\Omega/\sigma = 1$, (a) $\sigma t = 1$, (b) $\sigma t = 30$.

the probability density becomes rippled and develops multiple parallel filaments [see Fig. 2(b)]. The number of these filaments grows with time, and their width is diminishing in order to keep the occupied phase space volume constant. Eventually, all the filaments tend to become almost horizontal and uniform in density. As follows from Eq. (2), the neighboring filaments are separated in angular velocity by $2\pi/t$, where t is the evolution time.

At $t = T$, the ensemble is subject to another kick. Every filament in Fig. 2(b) is quite analogous to the initial uniform distribution of rotors shown in Fig. 1 by the blue line, but it has a nonzero mean velocity. With time, these filaments form the typical folded patterns leading to the transient orientation of the rotors in the filament. For every angle θ, the emerging patterns from neighboring filaments start moving with the velocity difference $2\pi/T$ with respect to each other. As a result, the kick-induced patterns are generally shifted with respect to each other most of the time after the kick, which results in a quasiuniform total angular distribution considered as a function of θ only. However, at time $\tau\sim T$ after the second kick, the folded filaments synchronously pile up near $\theta = 0$ due to the above "quantization" of the angular velocities of the strips [see Fig. 3(a)]. This results in an echo in the orientation factor $\langle\cos(\theta)\rangle$. Figure 3(b) demonstrates also orientation along $\theta = \pi$ that happens a little bit later in the same time region (antiorientation echo).

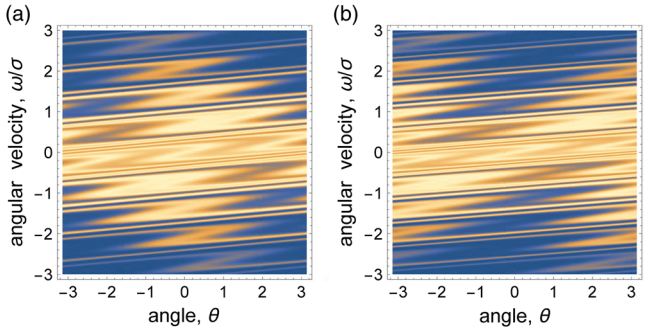

FIG. 3 (color online). Echo formation in the filamented phase space. $\Omega_1/\sigma = 1$, $\sigma T = 10$, and $\Omega_2/\Omega_1 = 1/3$. (a) $\sigma\tau = 9.11$—orientation echo. (b) $\sigma\tau = 10.85$—antiorientation echo.

These qualitative arguments have a considerable predictive power; in particular, the same mechanism should form the echo signals also at delays $2T, 3T, \cdots$ after the second pulse (higher-order echoes). Moreover, it is expected that synchronization of the patterns from non-neighboring strips at $\tau = T/2, T/3, \cdots$ causes highly symmetric structures in the phase space, which may be associated with "fractional echoes." These echoes are not seen in a mere orientation signal $\langle\cos(\theta)\rangle$, but require measuring higher-order observables $\langle\cos(n\theta)\rangle$ $(n > 1)$. Moreover, just looking at the phase space pattern at the moment of the main echo, Fig. 3(a), one may expect that the echo is best manifested if the delay T coincides with the time needed for achieving the maximal orientation in every strip. This means that for a given delay there exists a second-kick intensity that maximizes the echo signal.

The simple 2D model considered here [see Eq. (1)] allows for obtaining an analytical expression for the time-dependent mean value of $\langle\cos(n\theta)\rangle$, where n is an integer,

$$\langle\cos(n\theta)\rangle(\tau) = \sum_{k=0}^{k=\infty}(-1)^k e^{-\frac{1}{2}\sigma^2(n\tau-kT)^2} J_{k+n}(\Omega_2 n\tau) J_k\big(\Omega_1(n\tau - kT)\big). \tag{3}$$

For $n = 1, 2$ this quantity is the orientation factor and the alignment factor, respectively. Equation (3) presents a sequence of signals localized in time near $\tau = (k/n)T$, where k is an integer. For $n > 1$, these are the above mentioned fractional echoes, while $n = 1$ corresponds to the regular orientation echoes. Figure 4 presents the calculated time-dependent orientation factor for two values of the intensity of the second kick. In Fig. 4(a), the intensity of the second kick, Ω_2, was optimized to achieve the maximal amplitude of the main echo at $\tau \sim T$. Although the second kick in Fig. 4(a) is 3 times weaker than that of Fig. 4(b), it induces a considerably stronger echo, which even exceeds the initial response to the second kick. The peak and dip of the first echo in Fig. 4(a) correspond to Figs. 3(a) and 3(b), respectively. As follows from Eq. (3), the amplitude of the echo is a decaying oscillatory function of the intensity of the second kick, Ω_2, after reaching the global maximum shown at Fig. 4(a).

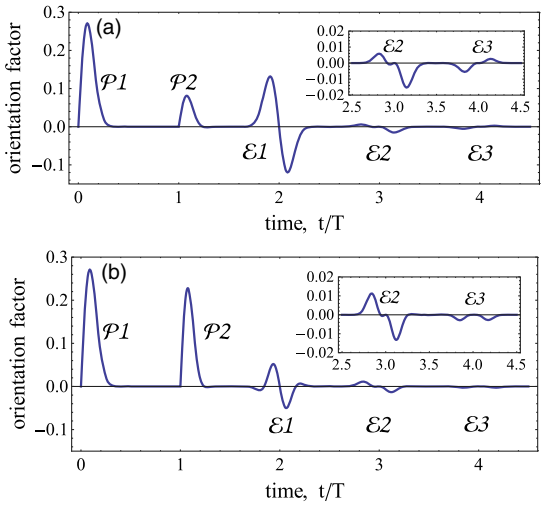

FIG. 4 (color online). Orientation factor versus time after the first kick. $\Omega_1/\sigma = 1$, $\sigma T = 10$. (a) $\Omega_2/\Omega_1 = 1/3$. (b) $\Omega_2/\Omega_1 = 1$. Here $\mathcal{P}1$ and $\mathcal{P}2$ denote transient responses to the first and the second kick, respectively. $\mathcal{E}1$, $\mathcal{E}2$, and $\mathcal{E}3$ are echoes of the first, second, and third order, respectively. Insets show a magnified view of the second and third echoes.

The same qualitative mechanism works in the case of the polarization-induced interaction $[V \sim -\cos^2(\theta)]$, and it produces echoes in the alignment signal $\langle\cos^2(\theta)\rangle(t)$. An analytical expression for the alignment echoes for 2D rotors is provided in the Supplemental Material [30], and it is quite similar to Eq. (3). The visualization of the phase space transformations in the case of alignment is more involved, but the main results remain the same, including the non-monotonous dependence of the echo signals on the intensity of the second kick.

We note the remarkable similarities between the physics of the laser-induced alignment or orientation of molecules [24–28] and modern techniques for laser manipulations over electron beams in accelerator-based light sources [11–14]. Both research fields aim at compressing the density of particles in certain areas (angular alignment or orientation versus electron bunching along the beam) by laser pulses, and in both cases phase-space folding is involved [11,14,29,31]. The orientation or alignment echoes described here have much in common with the phenomena involved in echo-enabled harmonics generation in free-electron lasers. This connection is not merely formal, and may be beneficial for both fields. In particular, recent proposals to use several laser fields to significantly increase the electrons' bunching factor [14] may be supported by a similar suggestion [29,31] in the context of molecular orientation or alignment by series of laser pulses. This concept was theoretically optimized [32], experimentally demonstrated [33–35], and even successfully applied to the enhanced focusing (bunching) of cold atoms interacting with multiple laser fields [36,37].

In what follows, we describe the first experimental observation of the rotational alignment echoes in laser-kicked CO_2 molecules. The details of our experimental setup [38] are described in the Supplemental Material [30]. The two linearly polarized pump pulses $\mathcal{P}1$ and $\mathcal{P}2$ are derived from an amplified Ti:sapphire laser (1 kHz, 800 nm, 100 fs FWHM) and properly delayed before being focused inside a CO_2 filled gas cell at a pressure of 0.2 bar. The alignment echoes are observed by time-resolved birefringence measurements [39], where a delayed, weak probe pulse, linearly polarized at +45° relative to the pump pulses is linearly analyzed after

passing through the cell by a polarizer set at −45° relative to the pump pulses. The birefringence signal measured on the detector can be written as [40]

$$\mathcal{S}(\tau) \propto \int_{-\infty}^{\infty} I_{\mathrm{pr}}(t-\tau)\left[\langle\cos^2(\theta)\rangle(t, I_1, I_2) - \frac{1}{3}\right]^2 dt, \qquad (4)$$

where $\langle\cos^2(\theta)\rangle(t, I_1, I_2)$ is the alignment factor, and I_1, I_2, and I_{pr}, are the intensity of $\mathcal{P}1$, $\mathcal{P}2$, and the probe pulse, respectively.

Figure 5 presents the pump-probe signals obtained for three different sets of pump intensities with a delay T between $\mathcal{P}1$ and $\mathcal{P}2$ set to 1.6 ps. We measured the alignment signals till about one half of the rotational revival time T_{rev} of the CO_2 molecule ($T_{\mathrm{rev}} \sim 42.7$ ps). The classical echo effects discussed in this Letter happen within the time interval of about $T_{\mathrm{rev}}/4$ where the alignment dynamics is well described by classical mechanics. To guide the eye, the alignment signals caused by the pulses $\mathcal{P}1$ and $\mathcal{P}2$, and also their one-quarter and one-half revivals, are colored in red and blue, respectively, whereas the echoes are highlighted with a yellow color. For each intensity set, an echo is produced after $\mathcal{P}2$ at $\tau \sim T$. Its amplitude depends on the intensities of both $\mathcal{P}1$ and $\mathcal{P}2$. The maximum echo amplitude seen in Fig. 5(c) is achieved for a second pulse that is weaker than the first one, $I_2/I_1 \sim 0.4$, and this echo is stronger than the initial response induced by the second pulse $\mathcal{P}2$. These observations resemble the theoretical results shown in Fig. 4, and they may be understood using the similar qualitative arguments. The second echo produced at $\tau \sim 2T$ is also visible in Fig. 5(c). On the longer time scale, replicas of these echoes are observed near the quarter- and half-revival regions. They appear due to the interplay between the classical echo effect and the phenomenon of fractional quantum revivals [41]. These replicas will not be discussed in detail here, but they are nicely reproduced in the fully quantum theoretical description of our experiments (to be published). Related transient signals were also reported in Ref. [42] where the alignment of N_2O molecules excited by two strong femtosecond laser pulses was studied. In these experiments the delay between the pulses was chosen close to the quarter-revival time, far beyond the region where the classical echo effects of the present Letter exist. In order to reveal the nonmonotonic dependence of the echo amplitude, we varied the intensity of the second pulse $\mathcal{P}2$ while keeping the first one ($\mathcal{P}1$) fixed. The results are summarized in Fig. 6, which demonstrates the existence of an optimal intensity of the second kick and the oscillatory dependence of the echo amplitude on this intensity, in agreement with our theoretical considerations.

Summarizing, we showed that a textbook classical system—a collection of randomly oriented free rotors with dispersed rotational velocities—exhibits multiple echoes of different kinds in its orientation or alignment dynamics when kicked by a pair of delayed pulses. We provided qualitative and quantitative analysis of the phenomenon using a simple model system, and performed the first

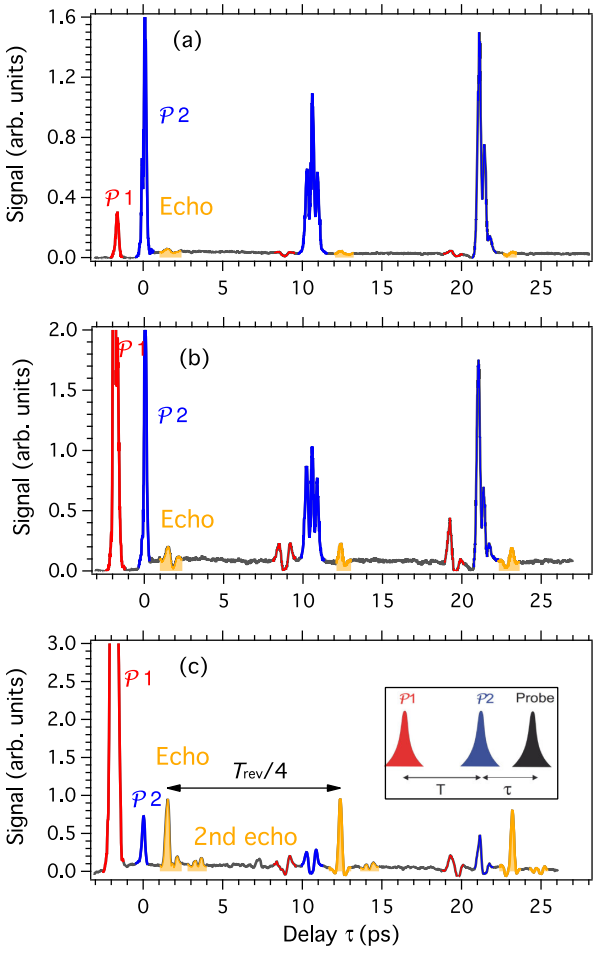

FIG. 5 (color online). Birefringence signals as a function of the pump-probe delay τ for different intensities I_1 and I_2 of the pump pulses $\mathcal{P}1$ and $\mathcal{P}2$, respectively (see the inset). T_{rev}: rotational revival time. (a) $I_1 = 15$ TW/cm^2, $I_2 = 38$ TW/cm^2. (b) $I_1 = 25$ TW/cm^2, $I_2 = 27$ TW/cm^2. (c) $I_1 = 38$ TW/cm^2, $I_2 = 15$ TW/cm^2.

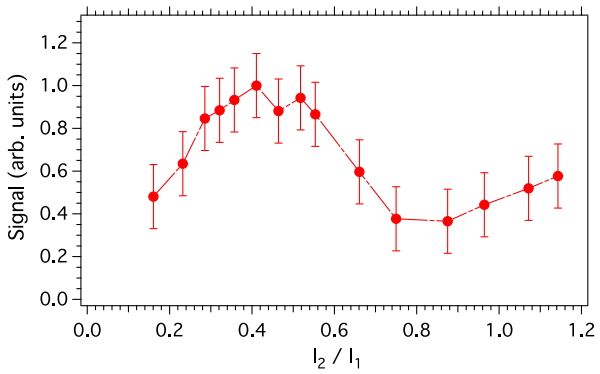

FIG. 6 (color online). Peak amplitude of the birefringence signal for the echo near $\tau = T$ versus I_2/I_1, with I_1 set to 44 TW/cm^2.

experimental demonstration of the classical alignment echoes in a thermal gas of CO_2 molecules excited by a pair of femtosecond laser pulses. The echoes were observed on a time scale much shorter than the quantum revival time, and their parameters were readily controllable by the intensity and delay of the excitation pulses. This makes the orientation or alignment echoes promising for exploring relaxation processes in high pressure gases and various liquids, including superfluid helium [43], where quantum rotational responses are considerably suppressed.

This work was supported by the Conseil Régional de Bourgogne (PARI program), the CNRS, the Labex ACTION program (Contract No. ANR-11-LABX-01-01), and the French National Research Agency (ANR) through the CoConicS program (Contract No. ANR-13-BS08-0013). This research was also supported by DFG (Project No. LE 2138/2-1) and Minerva Foundation. I. S. A. acknowledges the kind hospitality of and support from the Université Paris Est Créteil during a one week stay at LISA.

*olivier.faucher@u-bourgogne.fr
†ilya.averbukh@weizmann.ac.il

[1] E. L. Hahn, Phys. Rev. **80**, 580 (1950).
[2] R. M. Hill and D. E. Kaplan, Phys. Rev. Lett. **14**, 1062 (1965).
[3] R. W. Gould, Phys. Lett. **19**, 477 (1965).
[4] R. W. Gould, T. M. O'Neil, and J. H. Malmberg, Phys. Rev. Lett. **19**, 219 (1967).
[5] N. A. Kurnit, I. D. Abella, and S. K. Hartmann, Phys. Rev. Lett. **13**, 567 (1964).
[6] V. P. Chebotayev and B. Ya. Dubetsky, Appl. Phys. B **31**, 45 (1983).
[7] G. V. Stupakov, Echo Effect In Hadron Colliders, SSC Report No. SSCL-579, 1992.
[8] G. V. Stupakov and S. Kauffmann, Echo Effect in Accelerators, SSC Report No. SSCL-587, 1992.
[9] L. K. Spentzouris, J. F. Ostiguy, and P. L. Colestock, Phys. Rev. Lett. **76**, 620 (1996).
[10] O. Bruning, T. Linnecon, F. Ruggio, W. Scandale, and E. Shaposhnikova, *Nonlinear and Collective Phenomena in Beam Physics* (AIP, New York, 1997), p. 155.
[11] G. Stupakov, Phys. Rev. Lett. **102**, 074801 (2009).
[12] D. Xiang *et al.*, Phys. Rev. Lett. **105**, 114801 (2010).
[13] Z. T. Zhao *et al.*, Nat. Photonics **6**, 360 (2012).
[14] E. Hemsing, G. Stupakov, and D. Xiang, Rev. Mod. Phys. **86**, 897 (2014).
[15] G. Morigi, E. Solano, B.-G. Englert, and H. Walther, Phys. Rev. A **65**, 040102 (2002).
[16] T. Meunier, S. Gleyzes, P. Maioli, A. Auffeves, G. Nogues, M. Brune, J. M. Raimond, and S. Haroche, Phys. Rev. Lett. **94**, 010401 (2005).
[17] A. Bulatov, A. Kuklov, B. E. Vugmeister, and H. Rabitz, Phys. Rev. A **57**, 3788 (1998).
[18] F. B. J. Buchkremer, R. Dumke, H. Levsen, G. Birkl, and W. Ertmer, Phys. Rev. Lett. **85**, 3121 (2000).
[19] M. F. Andersen, A. Kaplan, and N. Davidson, Phys. Rev. Lett. **90**, 023001 (2003).
[20] M. Herrera, T. M. Antonsen, E. Ott, and S. Fishman, Phys. Rev. A **86**, 023613 (2012).
[21] G. Karras, E. Hertz, F. Billard, B. Lavorel, J.-M. Hartmann, O. Faucher, E. Gershnabel, Y. Prior, and I. Sh. Averbukh (to be published).
[22] R. W. Boyd, *Nonlinear Optics* (Academic Press, Boston, 1992).
[23] B. Friedrich and D. Herschbach, Phys. Rev. Lett. **74**, 4623 (1995); J. Phys. Chem. **99**, 15686 (1995).
[24] H. Stapelfeldt and T. Seideman, Rev. Mod. Phys. **75**, 543 (2003).
[25] Y. Ohshima and H. Hasegawa, Int. Rev. Phys. Chem. **29**, 619 (2010).
[26] S. Fleischer, Y. Khodorkovsky, E. Gershnabel, Y. Prior, and I. Sh. Averbukh, Isr. J. Chem. **52**, 414 (2012).
[27] M. Lemeshko, R. V. Krems, J. M. Doyle, and S. Kais, Mol. Phys. **111**, 1648 (2013).
[28] S. Pabst, Eur. Phys. J. Spec. Top. **221**, 1(2013).
[29] I. Sh. Averbukh and R. Arvieu, Phys. Rev. Lett. **87**, 163601 (2001).
[30] See Supplemental Material at http://link.aps.org/supplemental/10.1103/PhysRevLett.114.153601 for the analytical expression for the alignment echoes in the 2D model with the polarization-induced interaction, and for the details of the experimental setup.
[31] M. Leibscher, I. Sh. Averbukh, P. Rozmej, and R. Arvieu, Phys. Rev. A **69**, 032102 (2004).
[32] M. Leibscher, I. S. Averbukh, and H. Rabitz, Phys. Rev. Lett. **90**, 213001 (2003); Phys. Rev. A **69**, 013402 (2004).
[33] C. Z. Bisgaard, M. D. Poulsen, E. Péronne, S. S. Viftrup, and H. Stapelfeldt, Phys. Rev. Lett. **92**, 173004 (2004).
[34] K. F. Lee, I. V. Litvinyuk, P. W. Dooley, M. Spanner, D. M. Villeneuve, and P. B. Corkum, J. Phys. B **37**, L43 (2004).
[35] M. Renard, E. Hertz, S. Guérin, H. R. Jauslin, B. Lavorel, and O. Faucher, Phys. Rev. A **72**, 025401 (2005).
[36] M. Leibscher and I. Sh. Averbukh, Phys. Rev. A **65**, 053816 (2002).
[37] W. H. Oskay, D. A. Steck, and M. G. Raizen, Phys. Rev. Lett. **89**, 283001 (2002).
[38] G. Karras, E. Hertz, F. Billard, B. Lavorel, J.-M. Hartmann, and O. Faucher, Phys. Rev. A **89**, 063411 (2014).
[39] V. Renard, M. Renard, S. Guérin, Y. T. Pashayan, B. Lavorel, O. Faucher, and H. R. Jauslin, Phys. Rev. Lett. **90**, 153601 (2003).
[40] O. Faucher, B. Lavorel, E. Hertz, and F. Chaussard, in *Progress in Ultrafast Intense Laser Science*, Springer Series in Chemical Physics Vol. 100 (Springer, New York, 2011), Vol. II. pp. 79–108.
[41] I. Sh. Averbukh and N. F. Perelman, Phys. Lett. A **139**, 449 (1989).
[42] H. Jiang, C. Wu, H. Zhang, H. Jiang, H. Yang, and Q. Gong, Opt. Express **18**, 8990 (2010).
[43] D. Pentlehner, J. H. Nielsen, A. Slenczka, K. Mølmer, and H. Stapelfeldt, Phys. Rev. Lett. **110**, 093002 (2013).

Orientation and Alignment Echoes: Supplementary material

G. Karras[1], E. Hertz[1], F. Billard[1], B. Lavorel[1], J.-M. Hartmann[2], and O. Faucher[1*]
[1]*Laboratoire Interdisciplinaire CARNOT de Bourgogne, UMR 6303 CNRS-Université de Bourgogne, BP 47870, 21078 Dijon, France and*
[2]*Laboratoire Interuniversitaire des Systèmes Atmosphériques (LISA) CNRS (UMR 7583), Université Paris Est Créteil, Université Paris Diderot, Institut Pierre-Simon Laplace, Université Paris Est Créteil, 94010 Créteil Cedex, France*

Erez Gershnabel, Yehiam Prior, and Ilya Sh. Averbukh[†]
Department of Chemical Physics, The Weizmann Institute of Science, Rehovot 76100, Israel

ALIGNMENT ECHOES

Here we briefly summarize results for alignment echo in the systems that interact with electromagnetic field via the induced polarization (interaction potential $V \sim -\cos^2(\theta)$). The kick transformation describing the angular velocity, ω and angle θ of a rotor at time t after the first kick is given by Eq.(1) of the main text, in which $\sin(\theta_0)$ is replaced by $\sin(2\theta_0)$. By applying this transformation twice, we obtain the angular position of the rotor at time τ after the second kick that was applied at $t = T$:

$$\theta = \theta_0 + \omega_0 T - \Omega_1 T \sin(2\theta_0) + \tau \left\{\omega_0 - \Omega_1 \sin(2\theta_0) - \Omega_2 \sin\left[2(\theta_0 + \omega_0 T - \Omega_1 T \sin(2\theta_0))\right]\right\} \tag{S-1}$$

Using this expression, we calculate the time-dependent alignment factor

$$\langle \cos^2(\theta) \rangle = \frac{1}{2} + \frac{1}{2} \mathrm{Re} \langle e^{2i\theta} \rangle = \frac{1}{2} + \frac{1}{2(2\pi)^{3/2}} \mathrm{Re} \left[\int_{-\pi}^{\pi} d\theta_0 \int_{-\infty}^{+\infty} d\omega_0 e^{-\omega_0^2/(2\sigma^2)} e^{2i\theta} \right] \tag{S-2}$$

With the help of the well known formula

$$e^{iz\sin(\theta)} = \sum_{k=-\infty}^{k=+\infty} e^{ik\theta} J_k(z), \tag{S-3}$$

we expand $\exp\{-2i\tau\Omega_2 \sin\left[2(\theta_0 + \omega_0 T - \Omega_1 T \sin(2\theta_0))\right]\}$ in series of Bessel functions $J_k(2\Omega_2\tau)$, combine together all the terms proportional to ω_0 in the exponent, and perform the Gaussian integration. This yelds

$$\langle \cos^2(\theta) \rangle = \frac{1}{2} + \frac{1}{4\pi} \mathrm{Re} \sum_{k=-\infty}^{k=+\infty} J_k(2\Omega_2\tau) e^{-2\sigma^2[\tau-(k-1)T]^2} \int_{-\pi}^{\pi} d\theta_0 e^{-2i\Omega_1[\tau-(k-1)T]\sin(2\theta_0) - 2i(k-1)\theta_0} \tag{S-4}$$

We perform the remaining integration in (S-4) with the help of the inverse Fourier transform of Eq. (S-3), shift the summation index by 1, and neglect terms with the negative index (they are exponentially small if $\sigma T > 1$):

$$\langle \cos^2(\theta) \rangle = \frac{1}{2} + \frac{1}{2} \sum_{k=0}^{k=\infty} (-1)^k e^{-2\sigma^2[\tau - kT]^2} J_{k+1}[2\Omega_2\tau] J_k[2\Omega_1(\tau - kT)] \tag{S-5}$$

Expression (S-5) describes alignment echoes happening at $\tau \sim kT$ ($k = 1, 2, 3...$). The term for $k = 0$ describes the transient response just after the second pulse. The alignment factor (S-5) is very similar (up to the overall shift by 1/2, and rescaling the parameters) to the analytical expression for the orientation factor (3) in the main text. Therefore, all the qualitative properties of the echo signals discussed before for the orientation process, are applicable to the alignment process as well.

EXPERIMENTAL SETUP

A schematic representation of the experimental apparatus is presented in Fig. 1. The laser source is a Ti:Sapphire based, chirped-pulse amplified system delivering pulses centered at 800 nm with duration of 100 fs. The output pulses have a maximum energy of 3.5 mJ at 1 kHz repetition rate. A Mach-Zehnder interferometer generates two pump pulses $\mathcal{P}1$ and $\mathcal{P}2$ with a relative delay T adjustable through a computer controlled translation stage equipped with a corner cube reflector. These two pulses are linearly polarized in the same direction and focused inside a static cell using a plano-convex lens. The cell is filled with CO_2 molecules at room temperature under a pressure of 0.2 bar. The alignment echoes are observed by time-resolved birefringence measurements, a non-invasive method so far successfully applied to the detection of field-free molecular alignment [1]. A probe pulse is produced by inserting a beam splitter in the beam path just after the exit of the laser source. It is delayed using a second motorized translational stage, its energy is about two orders of magnitude lower than those of the pump pulses and its polarization is linear and set to $+45^\circ$ with respect to the polarization of the pump pulses. The transient molecular alignment induced by the pump pulses is revealed by the depolarization of the probe field recorded as a function of the delay τ between $\mathcal{P}2$ and the probe pulse. The depolarized field component is selected by a linear analyzer located after the cell and set at -45° with respect to the polarization of the pump pulses. The birefringence signal measured on the detector can be written as shown in Eq.(6) in the main text (see [2]). Finally, control over the energy of all beams is achieved using the combination of zero-order half wave-plates and Glan polarizers.

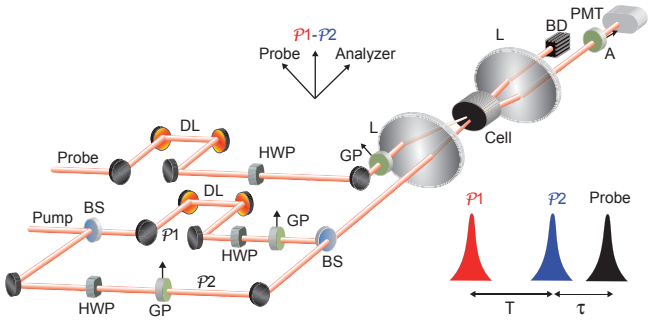

FIG. 1. (color online) Experimental set-up. A: Analyzer, BS: Beam Splitter, GP: Glan Polarizer, HWP: half wave-plate, PMT: Photo Multiplier Tube, L: Lens, DL: Delay Line, BD: Beam Dump. The relative polarizations of the different pulses together with the orientation of the analyzer along with a relative timing chart are shown in the insets. Here T is the delay between $\mathcal{P}1$ and $\mathcal{P}2$, and τ is the delay between $\mathcal{P}2$ and the probe pulse.

* olivier.faucher@u-bourgogne.fr
† ilya.averbukh@weizmann.ac.il

[1] V. Renard, M. Renard, S. Guérin, Y. T. Pashayan, B. Lavorel, O. Faucher, and H. R. Jauslin, Phys. Rev. Lett. **90**, 153601 (2003).
[2] O. Faucher, B. Lavorel, E. Hertz, and F. Chaussard, in it Progress in Ultrafast Intense Laser Science, vol. VII (Springer, 2011), vol. 100 of *Springer Series in Chemical Physics*, pp. 79-108.